Guided propagation of terahertz pulses on metal wires

Kanglin Wang and Daniel M. Mittleman

Department of Electrical and Computer Engineering, Rice University, Mail Stop 366, Houston, Texas 77251-1892

Received November 5, 2004; revised manuscript received April 7, 2005; accepted April 17, 2005

We demonstrate a new waveguiding structure for terahertz (THz) radiation in which broadband THz pulses are confined and guided along a bare metal wire. The propagation of THz pulses on such a waveguide is characterized with a fiber-coupled terahertz time-domain spectroscopy system. Free-space THz radiation is coupled onto the waveguide at different positions along the wire, and spatially resolved detection of the electric field of the guided wave is performed at the end of the wire. This waveguide exhibits the lowest attenuation of any waveguide for broadband THz pulses reported so far because of the minimal exposed metallic surface area. It also supports propagation of broadband radiation with negligible group-velocity dispersion, making it especially suitable for use in THz sensing and diagnostic systems. In addition, the structural simplicity lends itself naturally to the facile manipulation of the guided pulses, including coupling, directing, and beam splitting. These results can be described in terms of a model developed by Sommerfeld for waves propagating along the surface of a cylindrical conductor.

OCIS codes: 230.7370, 320.5390, 320.7160.

1. INTRODUCTION

Rapid advances in laser technology have enabled various techniques for the generation and detection of electromagnetic radiation in the terahertz (THz) region (spanning from ~100 GHz to ~10 THz).[1] As a result, numerous uses of THz radiation have been explored, including trace gas detection,[2] medical diagnosis,[3,4] security screening,[5] and defect analysis in complex materials such as Space Shuttle tiles.[6] Many of these studies have relied on THz time-domain spectroscopy (TDS), a technique used to generate subpicosecond pulses with spectral content spanning much of the THz band.[7–10]

However, progress is limited by the overwhelming reliance on free-space transport of the THz beam, by use of bulk optical components. In many real-world situations, the sample or region to be studied may not be readily accessible to a line-of-sight beam. Common devices such as optical fiber-based sensors or medical endoscopes rely on the guided-wave delivery of light to the remote sensing location. To extend this paradigm to THz applications, the development of optimized guided-wave devices is required. Furthermore, the development of practical THz waveguides will dramatically expand the application of THz TDS in areas such as gas sensing and nanometer thin-film measurements.[11,12]

The development of THz waveguides has been hindered by the material properties and the application requirements in this spectral range. The characteristics of materials at THz frequencies make it extremely difficult to build a fiber to guide THz beams over a long distance. The most transparent materials for this range are crystalline (e.g., high-resistivity silicon) and thus are costly, fragile, and challenging to form into specific geometries for waveguide configurations. Other materials, such as low-loss polymers or glasses, are more malleable but exhibit prohibitively high absorption losses for propagation distances of more than a few centimeters. For this reason, THz waveguides generally must rely on propagation in air, rather than by dielectric confinement as in an optical fiber. On the other hand, many THz applications rely on use of broadband pulses for time-domain analysis and spectroscopic applications. To avoid pulse reshaping during propagation, the significant additional constraint of low dispersion is also required. But for many conventional metal waveguides (e.g., metal tubes), pulse reshaping in propagation is difficult to avoid because of the extreme dispersion near the waveguide cutoff frequencies. Furthermore, finite conductivity of metals can lead to considerable losses in the wave propagation.

Great efforts have been devoted to finding useful THz waveguides within the past few years, and various guides with quasi-optical coupling have been demonstrated. Most of these THz waveguides have been based on conventional guiding structures, such as metal tubes,[11,13,14] plastic ribbons,[15] or dielectric fibers.[16] There have also been reports on the application of the latest technology of photonic crystal fibers to THz radiation.[17,18] In all these cases, the utility for transport of THz pulses is limited by group-velocity dispersion of the guided waves. The most promising studies have reported dispersionless propagation in parallel metal plate waveguides.[19–21] In this case the reported attenuation (~80 dB/m) is limited by the finite conductivity of the metal components.

In this paper we show how a metal waveguide with a simple geometry, namely, a bare wire, can be used to guide broadband THz pulses with outstanding performance, including low loss and negligible group-velocity dispersion. The guided propagation of THz pulses on a metal wire shows similar behavior to the transverse-electromagnetic (TEM) mode of a conventional coaxial waveguide[22] and also to the cylindrical surface guided waves first described by Sommerfeld.[23,24] Since the ex-

posed surface area of a wire is much smaller than that of any previously reported metal waveguide, the attenuation due to conductivity losses is extremely low for this configuration. As a result, the behavior is qualitatively different from that of many other metal guiding structures.[25] The structural simplicity of the wire waveguide presents great advantages in the manipulation of guided THz radiation.

2. PROPAGATION EFFECTS IN NEAR-FIELD OPTICAL ANTENNAS

The propagation of THz radiation along bare metal wires was first observed in the demonstration of apertureless near-field scanning optical microscopy (NSOM) using THz TDS. The experimental setup is depicted in the inset of Fig. 1. The broadband single-cycle pulses of free-space THz radiation are generated using a photoconductive transmitter and are focused onto a beryllium–copper probe acting as an apertureless near-field optical antenna. The probe has a tip of ~ 25 μm radius and a shaft of 0.5 mm diameter coated with a thin layer of tin to prevent oxidation. The sample is a featureless gold-coated silicon wafer, placed in close vicinity of the tip. The mean distance between the tip and the gold surface, $d \sim 350$ nm, is precisely controlled by a piezoelectric transducer. In such a configuration, the tip strongly interacts with its image in the metal surface and converts the localized evanescent field around the tip to propagating radiation through a scattering process.[26] The electric field of the scattered THz pulses is detected in the time domain by a photoconductive receiver that is located near the tip. In the measurement, the probe tip is vibrating normal to the surface at 750 Hz to modulate the scattered radiation, and the detected signal is demodulated using a lock-in amplifier. We can observe the propagation of THz pulses by moving the incident focal spot up along the shaft of the probe, as shown by the dashed arrow in Fig. 1. In this case, some of the incident THz radiation is coupled into a propagating mode on the shaft. This propagating mode moves down the shaft and excites the tip, producing a scattered wave that is detected by the receiver. Different incident positions lead to different propagation times and therefore different time delays in the detected time-domain waveforms. A piece of metal perpendicular to the needle is placed close to the shaft at the incident spot to provide a sharp start point of the propagation. Scattering of the THz radiation at the edge of this metal helps to couple the incident wave into a propagating mode on the shaft. The THz transmitter, the focusing lenses, and this metal scatterer are all mounted on a movable stage so that the incident position along the shaft can be precisely controlled.

The propagation effect is evident from the relative delay of the waveforms obtained by moving the transmitter stage along the shaft of the needle in steps of 1.5 mm.[27] As the point of incidence moves away from the tip, the pulse takes longer to propagate along the shaft, and its amplitude decreases. The propagation is largely nondispersive, since the shape of the time-domain waveform does not depend strongly on propagation distance. The group velocity of the propagation mode can be extracted from the time-domain waveforms. The relative time delay of these waveforms shows a linear dependence on the propagation distance, as depicted by the squares in Fig. 1. A least-squares fit to these data yields the group velocity $v_g = (3.00 \pm 0.01) \times 10^8$ m/s, the free-space velocity of light. A similar measurement is performed in which the needle is wrapped with a 0.5 mm polyvinyl chloride layer. The existence of the insulator layer distorts the detected waveforms and also reduces the group velocity of the propagation to $0.8c$, as depicted by the triangles in Fig. 1. This result indicates that the propagation is confined and guided along the surface of the probe.

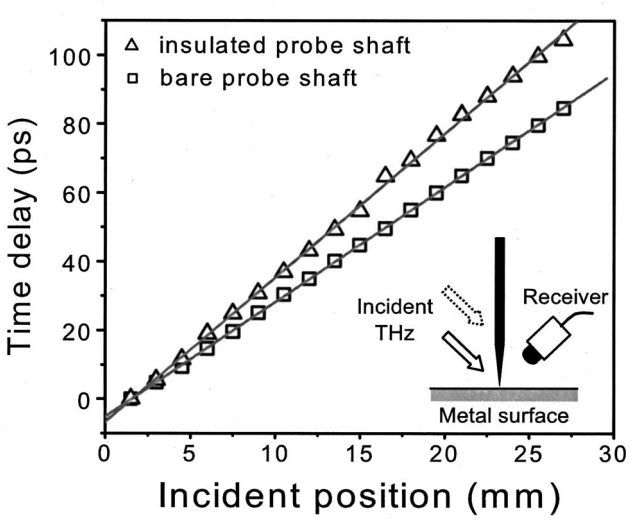

Fig. 1. Arrival time as a function of incident position for a series of time-domain THz pulses propagating along a bare metal probe (squares) and a probe wrapped with a 0.5 mm polyvinyl chloride insulation layer (triangles), detected in a THz apertureless near-field scanning optical microscopy system. The solid lines show the least-squares linear fit to these data, from which the group velocities can be obtained. The inset shows the experimental setup. Broadband THz pulses are focused onto a vibrating probe. The focal spot can be moved along the shaft of the probe. The propagating THz pulses are measured by detecting the scattered radiation from the probe tip with a photoconductive receiver.

In addition to the measurements with a bare needle and an insulated needle, we also performed the propagation measurements with a circular aluminum barrier situated on the probe and observed the disturbance and the reflection of the propagation mode.[27] These results have opened the possibility of a new method for THz waveguiding and manipulating. However, the waveforms we detect in these experiments are not the electric field of the propagating THz pulses, but the scattered radiation from the probe tip. To eliminate the spectral filtering effects introduced by the probe tip,[28] a new experimental configuration for direct measurement of the THz propagation on bare metal wires is required. This new configuration permits us to fully characterize the propagating mode along the wire waveguide.

3. DIRECT CHARACTERIZATION OF THE TERAHERTZ WIRE WAVEGUIDE

For a better observation and characterization of the guided THz propagation on metal wires, we change the

experimental setup from the NSOM configuration to a new configuration in which the electric field of the guided mode is directly detected at the end of the waveguide. With the fiber-coupled transmitter and receiver,[29] we can change the incident position (the start point of the propagation) and the detection position of the THz pulses to observe the spatial profile of the guided mode. We use a long stainless-steel wire with a smooth surface, rather than the tiny tapered probe in the NSOM experiments, as the waveguide for our new measurements.

A. Experimental Setup

The schematic of the new experimental setup is shown in Fig. 2. As in the NSOM experiments, the broadband single-cycle pulses of free-space THz radiation are generated and coherently detected using ultrafast photoconductive sampling.[7,8] The horizontally polarized THz pulses are focused onto the stainless-steel waveguide. Another stainless-steel wire is placed at the focal spot, oriented perpendicular to the waveguide (the y direction in Fig. 2). This second wire serves as an input coupler. Scattering of the input THz radiation at the intersection structure helps to excite the radially polarized mode that can propagate along the waveguide. Both the waveguide and the coupler are 0.9 mm in diameter, and the separation between them is 0.5 mm. The receiver is placed at the end of the waveguide and is oriented to detect only the vertically polarized component of the electric field to eliminate the possibility of detecting directly scattered radiation that would interfere with the detection of the guided mode. The incident THz beam is modulated by a chopper in front of the transmitter, and a lock-in amplifier is used to detect the induced photocurrent in the receiver. The THz transmitter, the focusing lenses, and the coupler are all mounted on a movable stage so that the incident position along the waveguide can be controlled. The THz receiver is mounted on a three-axis stage for detection at various positions with respect to the end of the waveguide.

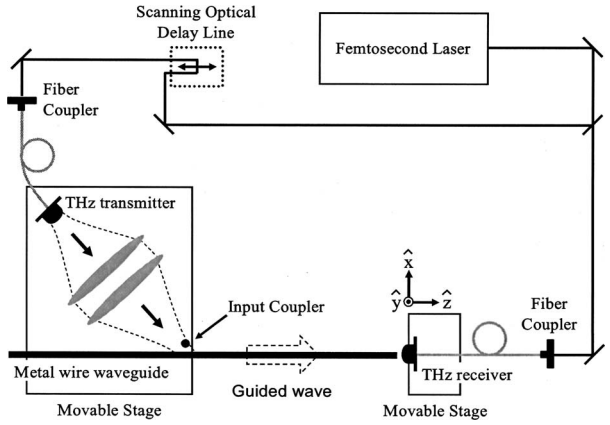

Fig. 2. Experimental setup for the direct characterization of the THz wire waveguide. Broadband THz pulses are generated by a fiber-coupled photoconductive transmitter and focused onto a stainless-steel waveguide with a diameter of 0.9 mm. A second stainless-steel wire is placed at the focal spot, oriented perpendicular to the waveguide, to act as an input coupler. The input THz beam is horizontally polarized, and the propagating mode excited around the wire waveguide is radially polarized. The electric field of the propagating mode is detected at the end of the waveguide with a fiber-coupled photoconductive receiver, which is sensitive only to the vertical polarization component. The transmitter, the focusing lenses, and the coupler are all mounted on a movable stage that can be moved along the waveguide. The receiver is mounted on a stage that can be moved in three dimensions with respect to the end of the waveguide.

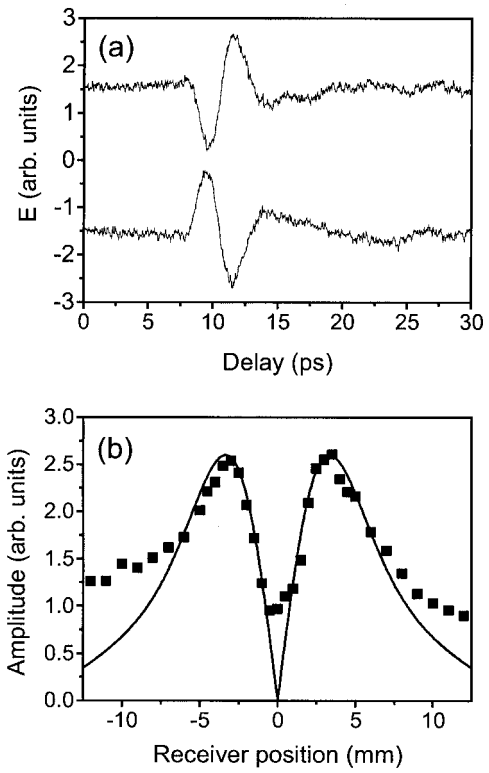

Fig. 3. Spatial profile of the propagating mode on a metal wire waveguide. (a) Time-domain electric field waveforms detected with the receiver 3 mm above and 3 mm below the waveguide. The polarity reversal shows the radial nature of the guided mode. (b) The amplitude of the THz pulses as a function of the vertical displacement of the receiver (squares), which is measured at a propagation distance of 24 cm. The solid curve shows the prediction of the Sommerfeld wave model described in the text, in which a Hankel function is convolved with a Gaussian of 6 mm full width at half-maximum to account for the finite aperture of the detector.

B. Spatial Profile

As the first step to characterize the propagating mode on the wire waveguide, we measure the spatial profile of the electric field around the waveguide by vertically scanning the THz receiver at the end of the waveguide. Figure 3(a) shows typical time-domain electric field waveforms for two different receiver positions located 3 mm above and 3 mm below the wire waveguide. These waves are vertically (y) polarized, perpendicular to the horizontally (x) polarized input beam. The polarity reversal as the detector scans across the wire clearly shows the radial nature of the guided mode. The peak-to-peak amplitude of the waveform as a function of the vertical displacement of the receiver is depicted by the squares in Fig. 3(b). The amplitude decreases with the transverse displacement approximately as $1/r$. Since the polarization response of the photoconductive receiver antenna is not perfectly symmetric, the measured electric field is not precisely zero at

the center point in the experiment. This can also explain the slight asymmetry in the amplitude profile of the detected waveforms.

The observed behavior can be understood in terms of either the TEM mode of a coaxial waveguide or in terms of a Sommerfeld wave. The TEM mode in a coaxial waveguide is radially polarized, and the electric field varies as the inverse of the radial position as

$$E_r = \frac{V}{r \ln \frac{a}{b}}, \tag{1}$$

where a and b are the radii of the outer and inner conductors, respectively, and V is a position-independent voltage.[22] Although providing a qualitative picture, this description cannot be extended to cover the case of interest here because this expression vanishes in the relevant limit, $a \to \infty$. A more accurate picture can be obtained from Sommerfeld's description of an electromagnetic wave propagating along the surface of a cylindrical conductor, a so-called Sommerfeld wire wave. In this case, it has been shown that the important propagating solution is an axially symmetric TM wave. Outside the metal, the variation of the radial electric field component (the dominant component) is described by a Hankel function $H_1^{(1)}(\gamma r)$, where γ is defined in terms of the propagation constant k of the field outside the wire according to $\gamma^2 = \omega^2/c^2 - k^2$. For a perfectly conducting wire, $\gamma = 0$ and the field propagates with a velocity determined solely by the external medium (in our case, air).[23] For large but finite conductivity, γ is small and the approximate form for the Hankel function can be used, appropriate for a small argument:

$$H_1^{(1)}(x) \approx -2i/\pi x. \tag{2}$$

Thus a Sommerfeld wire wave also exhibits $1/r$ decay, within a distance $r_0 \ll |1/\gamma|$ of the wire surface.

The Sommerfeld description can be used to estimate the distance that the wave extends from the metal surface for a metal of finite conductivity. To do so, one must determine γ by solving the transcendental equation that results from the boundary conditions at the wire surface. Following the method described by Goubau,[24] we compute the amplitude of the wave as a function of radial distance for the case of a 0.9 mm diameter stainless-steel (type 304) cylinder, with a conductivity of 1.39×10^6 mho/m, $\sim 2.4\%$ of the conductivity of copper. To account for the finite aperture of our detector, we convolve this Hankel function with a Gaussian of 6 mm full width at half-maximum. The resulting profile is shown as a solid curve in Fig. 3(b). We can also calculate the radius inside of which 50% of the power is guided. At a frequency of 0.3 THz, half of the power is transmitted through an area extending roughly 1.2 mm from the surface of the wire. The reasonably good agreement between the experimental results and the calculations suggests that the surface wave picture is an appropriate model for our experimental situation. However, as discussed in Subsection 3.C, the frequency-dependent attenuation is still lacking a quantitative description.

C. Propagation Characteristics

The propagation characteristics of the guided mode are studied by moving the incident position of the THz beam along the waveguide. In this way, we can obtain the time-domain waveforms as a function of propagation distance. There is no evident change in the temporal shape of the waveforms for propagation up to 24 cm, the limit of our optical delay line. This shows that the propagation is largely dispersionless. As in the NSOM experiment, we determine the broadband group velocity of the propagation mode by analyzing the dependence of the relative time delay of the waveforms on the propagation distance. A least-squares linear fit to these data yields the group velocity $v_g = (2.995 \pm 0.001) \times 10^8$ m/s, as shown in Fig.

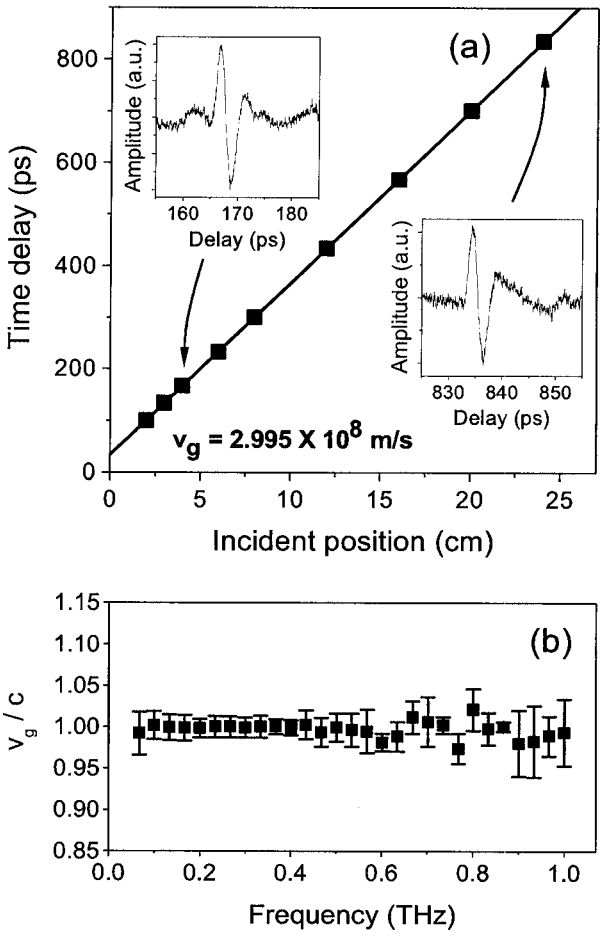

Fig. 4. Group velocity of the propagating THz pulses on a metal wire waveguide. (a) Arrival time as a function of incident position for a series of time-domain THz pulses detected using the setup illustrated in Fig. 2 (squares). The spectrum-weighted average group velocity of the guided mode is obtained from the least-squares linear fit to these data. The THz waveforms detected after 4 and 24 cm of propagation are shown in the insets. (b) Group velocity of the propagating mode as a function of frequency, derived from the spectra of the THz waveforms. No group-velocity dispersion is observed. This is consistent with the Sommerfeld wave model, in which the group velocity is predicted to vary by less than one part in 10^4 within the measured spectral range.

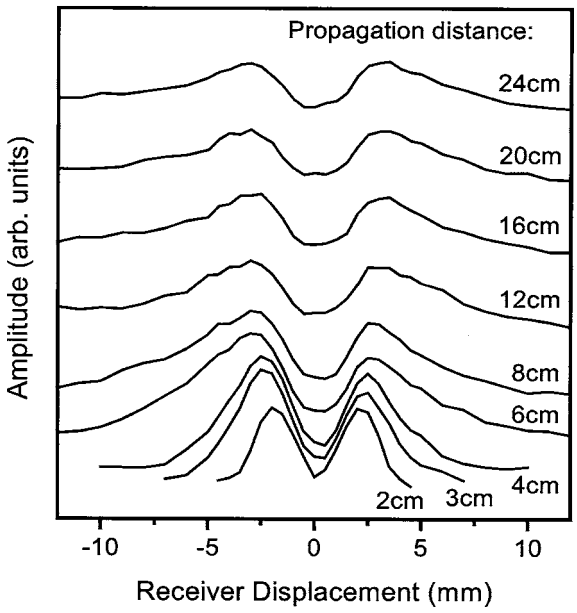

Fig. 5. Amplitude of the THz pulses as a function of the vertical displacement of the receiver, measured at different propagation distances. These curves sketch the spatial profile of the guided mode along the wire waveguide and show a lateral spreading of the guided mode.

4(a). To study the group-velocity dispersion, we extract the group velocity for different frequency components by analyzing the spectra of these waveforms using

$$v_g = \frac{c}{n_{\mathrm{eff}}(\omega) + \omega \dfrac{dn_{\mathrm{eff}}}{d\omega}}, \tag{3}$$

where n_{eff} is defined as

$$n_{\mathrm{eff}}(\omega) = \Delta\phi(\omega)\frac{c}{\omega d}. \tag{4}$$

$\Delta\phi(\omega)$ is the phase change for propagation distance d at angular frequency ω. Figure 4(b) shows the extracted data, confirming that there is no measurable group-velocity dispersion throughout the accessible spectral range. This is to be expected, given that the Sommerfeld surface wave model predicts a group velocity deviating from c by less than one part in 10^4 for our experimental situation.

To study the evolution of the guided mode in propagation, we compare the spatial profile of the guided mode detected at different propagation distances, each obtained in the same manner as that in Fig. 3(b). These profiles are depicted by the curves in Fig. 5. It is immediately clear that the electric field is more closely confined to the surface of the wire for the shortest propagation distances. Subsequently, the guided mode spreads laterally, especially during the first several centimeters of propagation, and approaches a spatial profile described roughly by $1/r$.

For each propagation distance, we extract the waveform with the maximum peak-to-peak amplitude. Except for the few shortest propagation distances, these are obtained at a fixed receiver offset of roughly 3 mm (see Fig. 5. These amplitudes are plotted as a function of propagation distance in Fig. 6(a). The amplitude attenuation coefficient α of the wire waveguide can be extracted from these data simply by fitting the dependence of the pulse amplitude E on the propagation distance x to

$$E(x) = E_0 \exp(-\alpha x). \tag{5}$$

The value we obtain, $\alpha = 0.03\ \mathrm{cm}^{-1}$, is the lowest of any waveguide for broadband THz pulses reported to date.[21] This method can give us the spectrum-weighted amplitude attenuation coefficient, but a more detailed characterization is required to obtain the frequency dependence of the loss. We extract the attenuation coefficient of each frequency component from the amplitude spectra of the

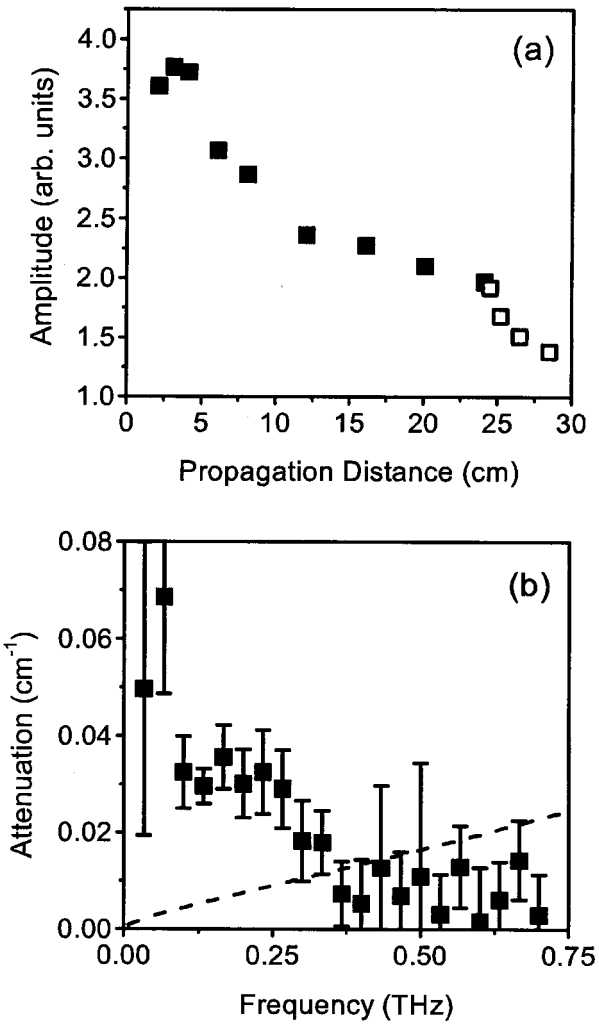

Fig. 6. Attenuation characteristic of the guided wave on a metal wire waveguide. (a) The maximum peak-to-peak amplitude of the THz pulses detected at each propagation distance (filled squares). Measurements with the receiver moved away from the end of the waveguide are also made (open squares), showing a sharp drop of the pulse amplitude as the radiation propagates off of the end of the waveguide into air. (b) The amplitude attenuation coefficient of the guided mode as a function of frequency, derived by analyzing the spectra of the THz waveforms detected at different propagation distances. In contrast to other terahertz waveguides, this loss decreases with increasing frequency. The dashed line shows the conductivity loss of the stainless-steel wire, computed using Sommerfeld's surface wave model.[24]

THz waveforms detected at various propagation distances. The spectrum of the attenuation coefficient is shown in Fig. 6(b). We note that the attenuation decreases with increasing frequency.

The low attenuation obtained here emphasizes one unique aspect of the wire waveguide. Compared with other waveguide geometries, a metal wire has a much smaller surface area interacting with the electromagnetic field, so the propagation loss due to finite conductivity of the metal is negligible.[22] This is consistent with Sommerfeld's wire wave model, which predicts a very small propagation loss due to the finite conductivity of the metal wire.[24] However, the spectrum of the attenuation obtained in our experiment cannot be described simply by the Sommerfeld model, as shown in Fig. 6(b). The predicted losses increase with increasing frequency, similar to other THz waveguides where the attenuation is dominated by ohmic effects.[20] In contrast, the observed losses decrease with increasing frequency. This indicates that much of the measured losses arises from other sources, such as diffractive spreading of the propagating mode in the lateral dimensions, as seen in Fig. 5. The significance of this loss mechanism for Sommerfeld waves has been discussed previously.[30] By moving the receiver away from the end of the waveguide, we observe a sharper drop in the amplitude of the detected pulses, as depicted by the open squares in Fig. 6(a), indicating an increasing divergence when the mode propagates off the end of the waveguide.

We note that our measurements do not reflect the losses associated with the coupling of the linearly polarized free-space THz beam to the guided mode. In the experiment described here, only ~1% of the power is coupled to the radially polarized waveguide mode from the free-space incident beam. More effective mode matching is needed to improve the input coupling.[31]

4. MANIPULATION OF THE GUIDED PULSES

We next explore the manipulation of the guided mode. The ability to direct radiation along curves is one of the most important features for a practical waveguide. We compare the amplitude of THz pulses after propagating on a waveguide bent with different radii. The results are shown by the open triangles in Fig. 7. The propagation distance is 21 cm, and the radius of curvature R is varied from 90 cm down to 20 cm in steps of 10 cm. The amplitude of the electric field E' as a function of the propagation distance x along the bent waveguide is described by

$$E'(x) = E_0 \exp(\alpha' x), \tag{6}$$

where α' is the amplitude attenuation coefficient for a bent waveguide. By comparing Eq. (6) with Eq. (5) we find

$$\alpha' = \alpha + \frac{\ln\left(\frac{E}{E'}\right)}{x}. \tag{7}$$

So the amplitude attenuation coefficient for each bend radius can be extracted by comparing the amplitude of the detected THz pulse with that of a straight waveguide with the same propagation distance x. The extracted data are depicted by the filled squares in Fig. 7. As we can see, even a slight bend on the waveguide can lead to a considerable increase in the loss, from 0.03 cm^{-1} for a straight waveguide to nearly 0.05 cm^{-1} for a bend radius of 90 cm.

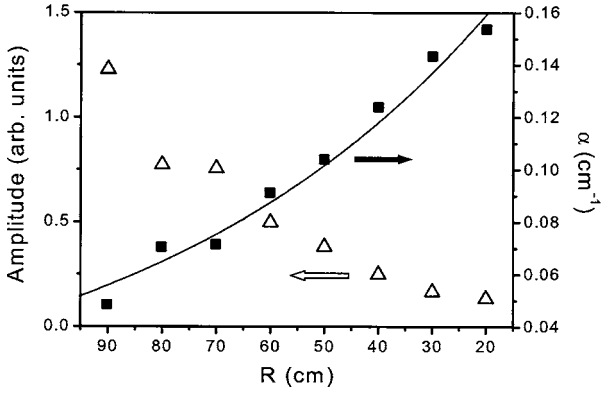

Fig. 7. THz wave propagation on a 21 cm long wire waveguide with different bend radii. The open triangles show the amplitude of the detected THz pulses as a function of the radius of curvature. The filled squares show the amplitude attenuation coefficient as a function of the radius of curvature. The data can be described by an exponential loss, as in a bent optical fiber. The fit is shown by the solid curve.

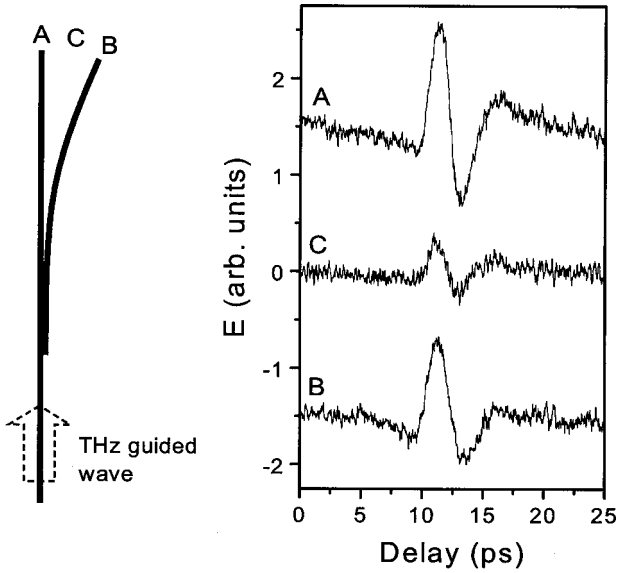

Fig. 8. A simple Y-splitter structure, consisting of a straight waveguide and a curved waveguide in contact with each other, as shown on the left. Part of the guided wave on the straight waveguide is coupled to the curved waveguide. THz waveforms detected at A, B, and C are shown on the right. The separation between A and B is 2 cm, and the THz receiver is located 3 mm below the plane of the splitter in these measurements.

The bend loss can be explained by the continuous conversion of the guided propagation into radiation modes as the wave travels around a curve. This is easy to understand by considering the wave front of the transverse field, which must rotate around the center of the curvature during propagation. Consequently, at some distance from the center of curvature the phase velocity would exceed c, the propagation speed of the guided mode. So the portion of the field outside this point must be radiated,

causing the power loss in the guided mode. This loss mechanism resembles that of a bent dielectric optical waveguide, in which the attenuation coefficient α can be described by a semiempirical form:[32]

$$\alpha = c_1 \exp(-c_2 R), \tag{8}$$

where R is the radius of curvature and c_1 and c_2 are constants independent of R. A fit with Eq. (8) shows good agreement with the experimental data, as seen in Fig. 7, suggesting that radiation is the dominant mechanism for the propagation loss of a bent metal wire waveguide.

From the spatial profile of the propagation [Figs. 3(b) and 5] we can see that the guided mode has a large extent compared to the cross section of the waveguide. So it is easy to imagine that the guided mode would be easily coupled between two curved waveguides in contact with each other (or between a curved waveguide and a straight one). These features enable a simple structure of a Y splitter for the wire waveguide, as illustrated in Fig. 8. The validity of this scheme has been verified by electric field measurements with such a structure. The waveforms in Fig. 8 are detected at the end of the straight waveguide (A), at the end of the curved waveguide (B), and at a position between them (C). The separation between A and B is 2 cm, and the waveforms are detected with the THz receiver 3 mm below the plane of the splitter structure. The plot clearly shows that part of the propagating power on the straight waveguide is directed to the branch waveguide by the Y splitter.

5. CONCLUSIONS

We have demonstrated a new type of THz waveguide with low loss, negligible group-velocity dispersion, and structual simplicity. This waveguide enables many new THz sensing applications. It is now possible to direct the THz pulse inside of containers or around corners, where line-of-sight optics are not practical. In addition to the waveguide described above, we have also tried many other metal wires as THz waveguides. The materials for these guides include steel, aluminum, copper, zinc, and nichrome. The wire diameter of these guides ranges from 0.5 to 6.4 mm. There is no strong difference in the performance of these waveguides, showing that THz pulses can be launched along any thin metal rod structures. In situations where the guided mode could be perturbed by other structures close to the waveguide, we could add a section of outer metallic shield to form a coaxial waveguide, as long as the additional ohmic losses can be tolerated.

With a Y-splitter structure used to separate the output wave from the input wave and a small mirror attached at the end of the waveguide as a 90 deg output director, we have successfully demonstrated a THz endoscope by detecting THz pulses reflected from the bottom and the side wall inside a container.[25] Further improvement could be made by combining an endoscope with an imaging system. This can be accomplished by scanning the endoscope along the surface of the detected region or, alternatively, scanning or rotating the sample to obtain an internal THz image. One challenge for this goal is the low power transmitted by the endoscope that strongly limits the data-acquisition rate as well as the dynamic range. With optimization of the mode of the input beam and the coupling geometry, the power launched into the endoscope probe can be greatly increased.[31]

It is also interesting to note that this waveguide naturally generates a radially polarized mode. So with a focusing lens mounted at the distal end of the endoscope, a higher resolution can be obtained than in the normal THz imaging system because of the sub-diffraction-limited focusing of radially polarized beams.[33,34] Furthermore, since the radially polarized mode is an ideal input field for a coaxial near-field probe[35–37] or an apertureless near-field optical antenna,[27] nanometer-resolved endoscopic THz imaging may be possible.[38] This will pave the way for a wide range of new applications for terahertz sensing and imaging.

ACKNOWLEDGMENTS

This work has been funded in part by the R. A. Welch Foundation, the National Science Foundation, and by Advanced Micro Devices.

The e-mail address for D. M. Mittleman is daniel@rice.edu.

REFERENCES

1. D. Mittleman, ed., *Sensing with Terahertz Radiation* (Springer-Verlag, 2002).
2. R. H. Jacobsen, D. M. Mittleman, and M. C. Nuss, "Chemical recognition of gases and gas mixtures with terahertz waves," Opt. Lett. **21**, 2011–2013 (1996).
3. R. M. Woodward, V. P. Wallace, D. D. Arnone, E. H. Linfield, and M. Pepper, "Terahertz pulsed imaging of skin cancer in the time and frequency domain," J. Biol. Phys. **29**, 257–261 (2003).
4. D. Crawley, C. Longbottom, V. P. Wallace, B. Cole, D. D. Arnone, and M. Pepper, "Three-dimensional terahertz pulse imaging of dental tissue," J. Biomed. Opt. **8**, 303–307 (2003).
5. K. Kawase, Y. Ogawa, and Y. Watanabe, "Non-destructive terahertz imaging of illicit drugs using spectral fingerprints," Opt. Express **11**, 2549–2554 (2003).
6. S. Wang and X.-C. Zhang, "Pulsed terahertz tomography," J. Phys. D **37**, R1–R36 (2004).
7. P. R. Smith, D. H. Auston, and M. C. Nuss, "Subpicosecond photoconducting dipole antennas," IEEE J. Quantum Electron. **24**, 255–260 (1988).
8. M. van Exter and D. Grischkowsky, "Characterization of an optoelectronic terahertz beam system," IEEE Trans. Microwave Theory Tech. **38**, 1684–1691 (1990).
9. P. U. Jepsen, R. H. Jacobsen, and S. R. Keiding, "Generation and detection of terahertz pulses from biased semiconductor antennas," J. Opt. Soc. Am. B **13**, 2424–2436 (1996).
10. D. M. Mittleman, R. H. Jacobsen, and M. C. Nuss, "T-ray imaging," IEEE J. Sel. Top. Quantum Electron. **2**, 679–692 (1996).
11. G. Gallot, S. P. Jamison, R. W. McGowan, and D. Grischkowsky, "Terahertz waveguides," J. Opt. Soc. Am. B **17**, 851–863 (2000).
12. J. Zhang and D. Grischkowsky, "Waveguide terahertz time-domain spectroscopy of nanometer water layers," Opt. Lett. **29**, 1617–1619 (2004).
13. R. W. McGowan, G. Gallot, and D. Grischkowsky, "Propagation of ultrawideband short pulses of THz radiation through submillimeter-diameter circular waveguides," Opt. Lett. **24**, 1431–1433 (1999).
14. J. A. Harrington, R. George, P. Pedersen, and E. Mueller, "Hollow polycarbonate waveguides with inner Cu coatings

for delivery of terahertz radiation," Opt. Express **12**, 5263–5268 (2004).
15. R. Mendis and D. Grischkowsky, "Plastic ribbon THz waveguides," J. Appl. Phys. **88**, 4449–4451 (2000).
16. S. P. Jamison, R. W. McGown, and D. Grischkowsky, "Single-mode waveguide propagation and reshaping of sub-ps terahertz pulses in sapphire fiber," Appl. Phys. Lett. **76**, 1987–1989 (2000).
17. H. Han, H. Park, M. Cho, and J. Kim, "Terahertz pulse propagation in a plastic photonic crystal fiber," Appl. Phys. Lett. **80**, 2634–2636 (2002).
18. M. Goto, A. Quema, H. Takahashi, S. Ono, and N. Sarukura, "Teflon photonic crystal fiber as terahertz waveguide," Jpn. J. Appl. Phys. Part 1 **43**, L317–L319 (2004).
19. R. Mendis and D. Grischkowsky, "Undistorted guided-wave propagation of subpicosecond terahertz pulses," Opt. Lett. **26**, 846–848 (2001).
20. R. Mendis and D. Grischkowsky, "THz interconnect with low loss and low group velocity dispersion," IEEE Microw. Wirel. Compon. Lett. **11**, 444–446 (2001).
21. S. Coleman and D. Grischkowsky, "A THz transverse electromagnetic mode two-dimensional interconnect layer incorporating quasi-optics," Appl. Phys. Lett. **83**, 3656–3658 (2003).
22. N. Marcuvitz, *Waveguide Handbook*, Massachusetts Institute of Technology Radiation Laboratory Series (McGraw-Hill, 1951).
23. J. A. Stratton, *Electromagnetic Theory* (McGraw-Hill, 1941).
24. G. Goubau, "Surface waves and their application to transmission lines," J. Appl. Phys. **21**, 1119–1128 (1950).
25. K. Wang and D. M. Mittleman, "Metal wires for terahertz wave guiding," Nature **432**, 376–379 (2004).
26. B. Knoll and F. Keilmann, "Near-field probing of vibrational absorption for chemical microscopy," Nature **399**, 134–137 (1999).
27. K. Wang, A. Barkan, and D. M. Mittleman, "Propagation effects in apertureless near-field optical antennas," Appl. Phys. Lett. **84**, 305–307 (2004).
28. K. Wang, D. M. Mittleman, N. C. J. van der Valk, and P. C. M. Planken, "Antenna effects in terahertz apertureless near-field optical microscopy," Appl. Phys. Lett. **85**, 2715–2717 (2004).
29. J. V. Rudd, D. Zimdars, and M. Warmuth, "Compact fiber-pigtailed terahertz imaging system," in *Commercial and Biomedical Applications of Ultrafast Lasers II*, J. Neev and M. K. Reed, eds., Proc. SPIE **3934**, 27–35 (2000).
30. Y. Xu and R. G. Bosisio, "Study of Goubau lines for submillimeter wave and terahertz frequency applications," IEE Proc., Part H: Microwaves, Antennas Propag. **151**, 460–464 (2004).
31. J. Deibel, M. Escarra, and D. M. Mittleman, "Photoconductive terahertz antenna with radial symmetry," Electron. Lett. **41**, 9–10 (2005).
32. R. Syms and J. Cozens, *Optical Guided Waves and Devices* (McGraw-Hill, 1992).
33. S. Quabis, R. Dorn, M. Eberler, O. Glöckl, and G. Leuchs, "Focusing light to a tighter spot," Opt. Commun. **179**, 1–6 (2000).
34. R. Dorn, S. Quabis, and G. Leuchs, "Sharper focus for a radially polarized light beam," Phys. Rev. Lett. **91**, 233–901 (2003).
35. U. C. Fischer and M. Zapletal, "The concept of a coaxial tip as a probe for scanning near field optical microscopy and steps towards a realisation," Ultramicroscopy **42**, 393–398 (1992).
36. F. Keilmann, "FIR microscopy," Infrared Phys. Technol. **36**, 217–224 (1995).
37. C. W. McCutchen, "Transmission line probes for scanning photon-tunneling microscopy," J. Scanning Microsc. **17**, 15–17 (1995).
38. H.-T. Chen, R. Kersting, and G. C. Cho, "Terahertz imaging with nanometer resolution," Appl. Phys. Lett. **83**, 3009–3011 (2003).